THE JOURNAL OF BIOLOGICAL CHEMISTRY VOL. 280, NO. 46, pp. 38767–38775, November 18, 2005

Structural Analysis of a HAMP Domain

*THE LINKER REGION OF THE PHOTOTRANSDUCER IN COMPLEX WITH SENSORY RHODOPSIN II**

Received for publication, August 25, 2005, and in revised form, September 9, 2005 Published, JBC Papers in Press, September 12, 2005, DOI 10.1074/jbc.M509391200

Enrica Bordignon[‡1], Johann P. Klare[§1], Meike Doebber[‡], Ansgar A. Wegener[§2], Swetlana Martell[§], Martin Engelhard[§3], and Heinz-Jürgen Steinhoff[‡4]

From the [‡]Fachbereich Physik, Universität Osnabrück, Barbarastrasse 7, 49069 Osnabrück and [§]Max-Planck-Institut für Molekulare Physiologie, Otto-Hahn-Strasse 11, 44227 Dortmund, Germany

Sensory rhodopsin II, the photophobic receptor from *Natronomonas pharaonis* (NpSRII)[5], forms a 2:2 complex with its cognate transducer (*N. pharaonis* halobacterial transducer of rhodopsins II (NpHtrII)) in lipid membranes. Light activation of NpSRII leads to a displacement of helix F, which in turn triggers a rotation/screw-like motion of TM2 in NpHtrII. This conformational change is thought to be transmitted through the membrane adjacent conserved signal transduction domain in histidine kinases, adenylyl cyclases, methyl-accepting chemotaxis proteins, and phosphatases (HAMP domain) to the cytoplasmic signaling domain of the transducer. The architecture and function of the HAMP domain are still unknown. In order to obtain information on the structure and dynamics of this region, EPR experiments on a truncated transducer ($NpHtrII_{157}$) and NpSRII, site-directed spin-labeled and reconstituted into purple membrane lipids, have been carried out. A nitroxide scanning involving residues in the transducer helix TM2, in the predicted AS-1 region, and at selected positions in the following connector and AS-2 regions of the HAMP domain has been performed. Accessibility and dynamics data allowed us to identify a helical region up to residue Ala^{94} in the AS-1 amphipathic sequence, followed by a highly dynamic domain protruding into the water phase. Additionally, transducer-transducer and transducer-receptor proximity relations revealed the overall architecture of the AS-1 sequences in the 2:2 complex, which are suggested to form a molten globular type of a coiled-coil bundle.

Phototaxis in halophilic Archaea is mediated by two sensory rhodopsins, SRI and SRII (also named phoborhodopsin (1)), which structurally and functionally are closely related to the two light-driven ion pumps bacteriorhodopsin and halorhodopsin (2, 3). The photophobic receptor SRII is tightly bound to its cognate transducer protein HtrII, which exhibits a transmembrane and a cytoplasmic signaling domain, connected via a linker region including a HAMP[5] domain (4, 5) (see Fig. 1). This is suggested to be a conserved signal transduction domain identified in histidine kinases, adenylyl cyclases, methyl-accepting chemotaxis proteins, and phosphatases (4).

The transmembrane N-terminal domain consists of two transmembrane helices (TM1 and TM2) and comprises part of the receptor-binding site. The x-ray crystallographic structure (6) of the complex formed by SRII and a C-terminal truncated HtrII from *Natronomonas pharaonis* revealed the close interaction between the transducer transmembrane helices and the receptor helices F and G. No structural data are available for the transducer beyond position 82.

Based on primary sequence homologies, the HAMP domain is predicted to consist of two helical amphipathic sequences (AS-1 and AS-2) linked by a connector sequence of undefined secondary structure (Fig. 1) (7). Despite many efforts, there are no structural or functional data available for any of the HAMP domains.

The long rod-shaped cytoplasmic domain of the transducer, which is suggested to be arranged in a four-helix bundle in analogy to the chemoreceptors Tsr and Tar from *Escherichia coli* (8), harbors the signaling domain involved in the signal transfer to the His kinase CheA and the methylation sites implicated in adaptation processes to constant stimuli. As shown previously (9, 10), a chimeric fusion protein consisting of SRII fused to an HtrII C-terminally truncated from *N. pharaonis* joined to the cytoplasmic domain of *E. coli* chemotaxis receptor Tsr is able to perform photosignaling activity, thus further supporting a common design for the two cytoplasmic signaling domains.

Previous SDSL EPR studies (11–13) suggested that the transduction of the signal is triggered by a light-induced movement of helix F, which in turn induces a rotary/screw-like motion of the transducer helix TM2. How this TM2 movement, which has been proven so far in the transmembrane transducer region (positions 78–82), is subsequently propagated along the cytoplasmic rod to the CheA-binding site is still a matter of debate.

Complexed to NpHtrII, the receptor NpSRII is no longer capable of light-driven proton pumping (14, 15). This observation has been utilized in a study (16) applying calorimetric and electrophysiological methods to identify the cytoplasmic portion of the receptor binding domain of NpHtrII. It was shown that an N-terminal sequence of 114 amino acids is sufficient for tight binding and for blocking of the proton pump. The cytoplasmic portion of the transducer, which is responsible for the inhibition of the proton pump, is located in the connector region of the HAMP domain (Fig. 1). Recent studies on the linker region of NpHtrII (17) and HtrI (18) (corresponding to positions 87–95, numbering according to NpHtrII) revealed initial insight into the topology of

* This work was supported by a research fellowship from the Alexander von Humboldt Stiftung (to E. B.), Grant SFB 431/P18 from the Deutsche Forschungsgemeinschaft (to M. E., E. B., and H.-J. S.), and the Max Planck Society (to M. E.). The costs of publication of this article were defrayed in part by the payment of page charges. This article must therefore be hereby marked "*advertisement*" in accordance with 18 U.S.C. Section 1734 solely to indicate this fact.

[1] Both authors contributed equally to this work.
[2] Present address: Merck KGaA Darmstadt, Dept. of Gene Expression and Biotechnology, Frankfurter Strasse 250, 64293 Darmstadt, Germany.
[3] To whom correspondence may be addressed. Tel.: 49-231-1332302; E-mail: martin.engelhard@mpi-dortmund.mpg.de.
[4] To whom correspondence may be addressed. Tel.: 49-541-9692675; E-mail: hsteinho@uos.de.

[5] The abbreviations used are: HAMP domain, conserved signal transduction domain in histidine kinases, adenylyl cyclases, methyl-accepting chemotaxis proteins, and phosphatases; NpSRII, *Natronomonas pharaonis* sensory rhodopsin II; $NpHtrII_{157}$, *Natronomonas pharaonis* halobacterial transducer of rhodopsins II, truncated at residue 157; PML, purple membrane lipids; SDSL site directed spin labeling; mT, millitesla; CrOx, chromium oxalate.

the membrane proximal domain of the transducer with respect to the receptor in the solubilized complex.

We report here the use of SDSL EPR to investigate the structure and the overall architecture of the HAMP domain in the 2:2 complex. Residues in the transducer helix TM2 (Val^{78}–Leu^{82}) and those succeeding this helix in the predicted helical amphipathic sequence AS-1 (Gly^{83}–Gly^{101}) were mutated to cysteines and subsequently coupled to the methanethiosulfonate spin label. Additionally, four residues in the negatively charged region connecting AS-1 to AS-2 (Leu^{105}, Asp^{106}, Asp^{115}, and Glu^{116}), one in the AS-2 region (Ala^{122}), and one close to the C-terminal end of $NpHtrII_{157}$ (Ala^{148}) have been investigated (Figs. 1 and 2). The topology of the complex at the level of the transducer linker region has been elucidated by using four parameters addressable by EPR spectroscopy: the mobility of the spin label side chains R1; their orientation toward buffer, lipid, or protein interior; the polarity of their environment; and distances between two spin labels.

EXPERIMENTAL PROCEDURES

Bacterial Strains—E. coli XL1 was used as a host for DNA manipulations. Gene expression was carried out *in E. coli* BL21 (DE3).

Cysteine Mutants—Starting with the plasmids pET27bmod-npsopII-His (19) and pET27bmod-$nphtrII_{157}$-His (C-terminally truncated transducer (1–157)) (12), cysteine encoding mutations were introduced by using the overlap extension method as described previously (20). The final PCR products were ligated into pET27bmod by using the NcoI and HindIII restriction sites. Positive clones were verified by DNA sequencing.

Protein Expression and Spin Labeling—NpSRII-His, $NpHtrII_{157}$-His, and respective cysteine mutants were expressed in *E. coli* BL21 (DE3) according to Shimono *et al.* (21) and purified as described in Hohenfeld *et al.* (19). The methanethiosulfonate spin label (the corresponding side chain is also abbreviated as R1; TRC, Toronto, Canada) was covalently attached to the cysteine residues of the solubilized NpSRII-His or $NpHtrII_{157}$-His mutants as outlined by Pfeiffer *et al.* (22). Excess label was removed by DEAE chromatography. For preparation of the complex, both components were isolated independently and mixed in a 1:1 molar ratio. For reconstitution into purple membrane lipids (PML), the mixtures were shaken (16 h at 4 °C in the dark) in a buffer (1 M NaCl, 10 mM Tris, pH 8) containing a 40-fold excess of lipids and detergent-absorbing Biobeads (SM2; 10 mg/mg dodecyl maltoside; Roche Applied Science). After filtration, the reconstituted protein-containing membranes were pelleted by centrifugation at 100,000 × *g* and resuspended in 150 mM NaCl, 10 mM Tris, pH 8.

EPR Measurements—Room temperature continuous wave EPR spectra were recorded using a homemade EPR spectrometer equipped with a Bruker dielectric resonator, with the microwave power set to 0.4–0.6 milliwatt, and B-field modulation amplitude adjusted to 0.15 mT. Samples were loaded into EPR glass capillaries (0.9 mm inner diameter) at final concentrations of 15–20 mg/ml (sample volume 15 μl).

EPR spectra for interspin distance determination were recorded at 160 K using a homemade EPR spectrometer equipped with an AEG H103 rectangular cavity. The magnetic field was measured with a B-NM 12 B-field meter (Bruker). A continuous flow cryostat Oxford ESR 900 allowed stabilization of the sample temperature. The microwave power was set to 0.2 milliwatt and the B-field modulation amplitude adjusted to 0.25 mT. Samples were loaded into EPR quartz capillaries (3-mm inner diameter) at final concentrations of 15–20 mg/ml protein (sample volume 40 μl).

The accessibility for paramagnetic quenchers, Π, was quantified by the method of continuous wave power saturation (23, 24). The EPR spectrometer equipped with the Bruker dielectric resonator was used; microwave power from 0.1 to 30–40 milliwatts was applied to the sample. The protein sample was loaded into a gas-permeable TPX capillary (Spintec). The sample was deoxygenated by a nitrogen gas flow around the capillary for the reference measurements; for oxygen-accessibility measurements nitrogen was replaced by air (21% O_2); for water-accessibility measurements a chromium oxalate (CrOx) solution was added to the same sample to a final concentration of 50 mM, and the nitrogen gas flow was restored. In case of high accessibility values, the measurements were repeated with 25 mM CrOx to minimize errors in the fitting procedure. The accessibility values obtained were then multiplied by 2 to obtain the expected values for 50 mM CrOx. Prior to EPR experiments, the sample was fluxed with the proper gas for 20 min. The errors of the Π values were determined to be in the range of ±10%.

For positions 95–101, accessibility experiments using the neutral Ni-ethylene diamine-N,N′-diacetic acid (20 mM) as a paramagnetic relaxing agent were also performed. No differences were observed between the trends of Π values obtained with the two water-soluble relaxing agents.

Fitting of Simulated EPR Spectra—Fitting of simulated dipolar broadened EPR powder spectra to the experimental ones detected at 160 K was performed according to the method described in detail by Steinhoff and co-workers (25). Because of the flexible spin label side chain, a random distribution of nitroxide ring orientation with respect to the interspin distance vector is assumed. To account for a range of distances expected to arise from these different orientations, a Gaussian distribution of interspin distances with 0.2 nm width is allowed. During the fitting procedure, the *g* tensor values, two components of the *A* tensor, and the line width parameters were fixed according to the values found from analysis of the corresponding singly labeled species. For the spin-labeled transducer in the reconstituted complex, this was achieved with a 1:4 labeled/unlabeled mixture that leads to a negligible amount of doubly labeled dimers in the sample or with the solubilized form of the complex that leads to the disruption of the dimer. For the spin-labeled receptor, the singly labeled mutants in the reconstituted or solubilized form were considered. The analysis of several singly labeled mutants allows us to obtain the fitting parameters suitable for the fit of all the spectra. The spectrum of the solubilized NpSRII/NpHtrII-A94R1 was chosen as the reference spectrum without dipolar broadening (Fig. 6). The parameters used are $g_{xx} = 2.0086$, $g_{yy} = 2.0066$, $g_{zz} = 2.0026$, $A_{xx} = 0.52$ mT, $A_{yy} = 0.45$ mT, and A_{zz} was variable to account for different polarity of the spin label environment (12, 26, 27). The spectra were convoluted with a field-independent line shape function composed of a superposition of 44% Lorentzian and 56% gaussian of 0.3 and 0.39 mT, respectively. The fitting parameters for the determination of the dipolar broadening are thus the average interspin distance, the fraction of the singly labeled component, and A_{zz}. The fraction of the singly spin-labeled component has been estimated from spin labeling efficiency calculations performed on the investigated mutants to be in the range of 40%.

Fitting of simulated EPR spectra to the experimental ones detected between 278 and 308 K (Fig. 5) was performed according to the Brownian model of isotropic reorientational diffusion (28). The rotational correlation times for the two spectral components were allowed to vary with temperature. The obtained ratio of the two spectral components was used to calculate the thermodynamic parameters in terms of a simple thermodynamic equilibrium between two conformations.

RESULTS

The nitroxide scanning was performed on samples covering the first predicted helix of the HAMP domain (AS-1). Additionally, residues in

FIGURE 1. **Primary sequence comparison of HAMP domains from different sensory proteins.** Sequences of HtrII were from *N. pharaonis* (investigated in this study, residues subjected to SDSL EPR analysis are *boxed* in *red*); HtrI and HtrII were from *Halobacterium salinarum*; four methyl-accepting chemotaxis proteins and a putative diguanylate cyclase/phosphodiesterase (YhjK) were from *E. coli*. The estimated limits of the two amphipathic sequences (AS-1 and AS-2) and the connector are indicated at the *bottom*. Heptad repeats of helices predicted from secondary structure analysis (according to Ref. 7) are denoted by *letters a–g*. Positions *a* and *d*, usually occupied by hydrophobic residues, are shown in *boldface*. Putative helix breaking elements in the 83–89 region are highlighted in *yellow*. The numbering corresponds to the NpHtrII sequence.

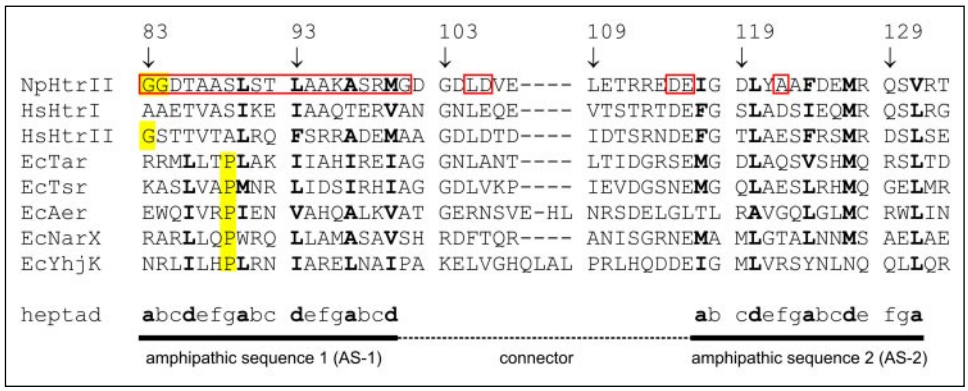

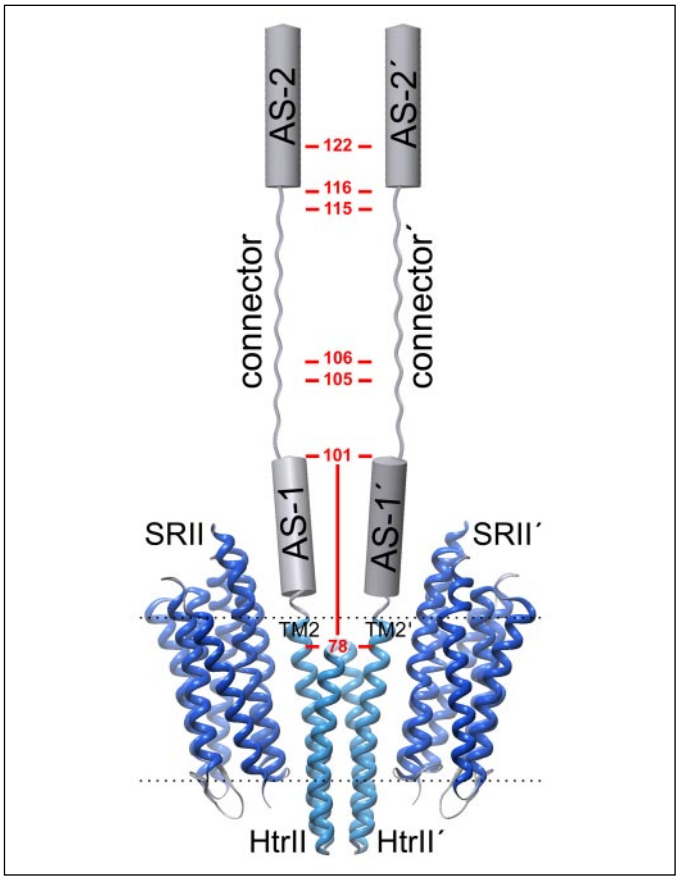

FIGURE 2. **Schematic representation of the predicted AS-1-connector-AS-2 sequence in the 2:2 NpSRII-NpHtrII complex.** The *colored ribbon* represents the x-ray structure (1H2S protein data bank (6)) of the transmembrane domain of the complex (NpSRII, *blue*; NpHtrII, *cyan*); a schematic representation of the HAMP sequence protruding perpendicularly to the membrane plane into the cytoplasmic phase is depicted in *gray*. For the sake of clarity, the predicted α-helical sequences AS-1 and AS-2 (*gray cylinders*) and the extended connector region (*gray line*) are proportionally stretched according to the length of the sequence. The two putative helix breaking residues Gly^{83} and Gly^{84} are represented as the *gray lines* connecting the helices TM2 to the AS-1 cylinders. Positions subjected to the SDSL EPR study are indicated in *red*.

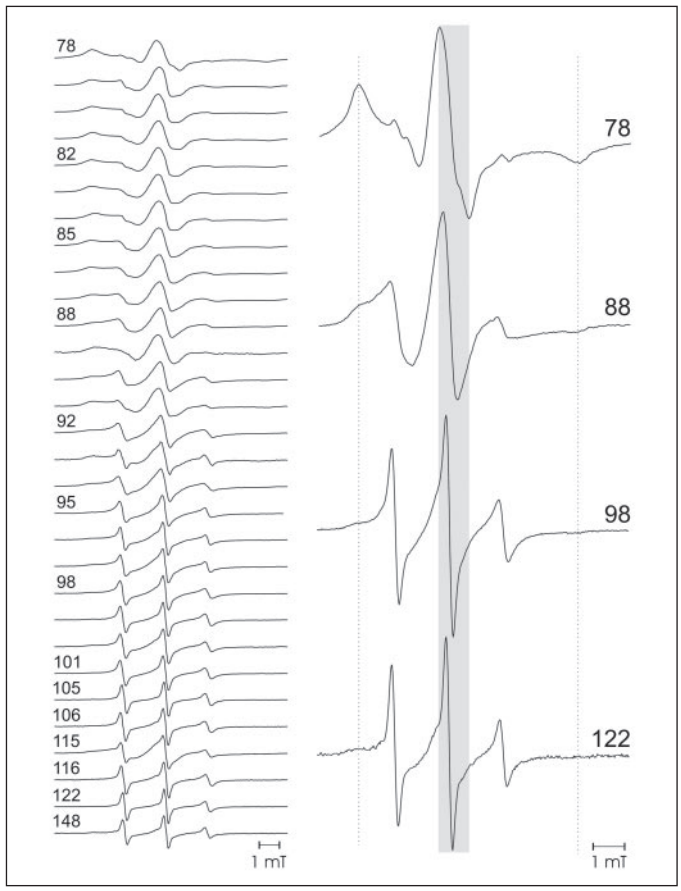

FIGURE 3. **Room temperature continuous wave X-band EPR spectra of the investigated spin-labeled $NpHtrII_{157}$ in complex with NpSRII reconstituted in PML scaled to equal (positive) amplitude of the central resonance peak.** The spin-labeled mutants are designated by the residue number at which the nitroxide is introduced. The *right panel* represents selected EPR spectra characterized by different mobility of the spin label, low (*78*), intermediate (*88*), and high (*98* and *122*), respectively. The *gray box*, indicating the central resonance line width, ΔH_0^{-1}, of the V78R1 spectrum is drawn to guide the eyes to better visualize the decrease of the line width observed. The *vertical dotted lines* indicate the low and high field hyperfine extremes characterizing the immobilized nitroxide of V78R1.

the connector and in the AS-2 sequence were chosen in order to determine the inter-relationship and connectivity of the transducer molecules in the 2:2 complex (see Figs. 1 and 2).

In a first set of experiments, the spin label side chain mobility and accessibility are determined. The temperature effects on the spectral features are analyzed, and finally interspin distances are determined between the two transducers as well as between the transducer and the receptor.

Analysis of Side Chain Mobility and Accessibility—The room temperature X-band EPR spectra detected for the spin-labeled residues in the NpSRII-HtrII complex reconstituted in PML are presented in Fig. 3. The majority of the EPR spectra detected presents a composite spectral shape, revealing the presence of at least two components that could arise, as noted previously by Hubbell *et al.* (29), from inhomogeneous structural constraints in the protein environment surrounding the label. It is evident that moving from the transducer transmembrane region

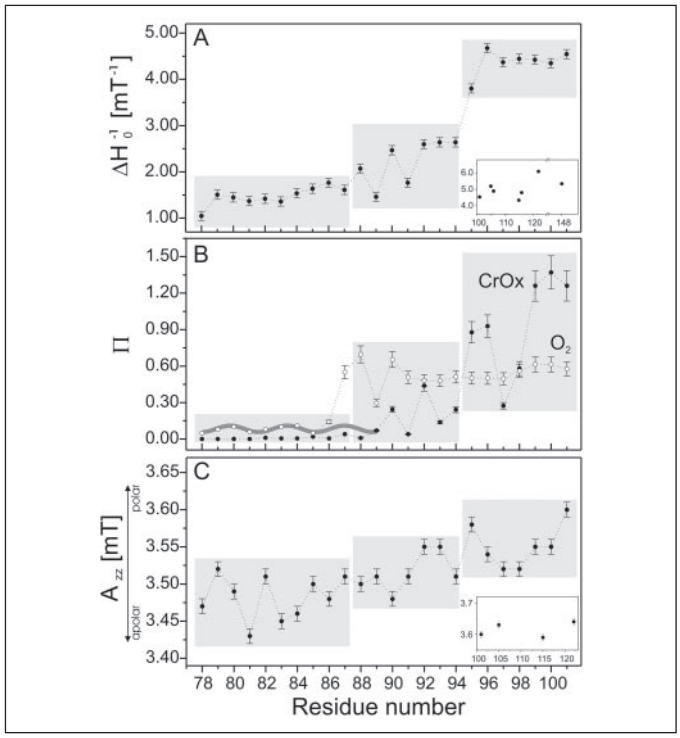

FIGURE 4. **Spectral parameters *versus* residue number of spin-labeled NpHtrII$_{157}$ in complex with NpSRII reconstituted in PML.** *A,* mobility parameter ΔH_0^{-1}; the estimated error is ± 0.01 mT^{-1} due to the uncertainties of the line width determination in the presence of multiple components. The boundaries between the three observed segments in the AS-1 sequence (*shaded* in *gray*) are empirical and taken from Hubbell *et al.* (29). The mobility parameters for the additional positions investigated in the connector region and in the AS-2 sequence are presented in the *inset*; for better comparison the value obtained for position 101 is also included. *B,* accessibility parameters Π_{Oxygen} (*open circles*) and Π_{CrOx} (*close circles*). The Π_{Oxygen} values are measured in the presence of air (21% O_2) and scaled to 100% oxygen. The *gray line* highlights the 3.6 periodicity. *C,* polarity parameters (A_{zz}) determined from the fitting of simulated spectra to the experimental ones at 160 K. The A_{zz} values determined for the positions investigated in the connector region and in the AS-2 sequence are presented in the *inset*; for better comparison the value obtained for position 101 is also included. The three segments identified from the analysis of the mobility parameters are visible in all profiles.

toward the predicted AS-1 domain up to position 101 that the EPR spectra show a gradual decrease of the spectral line widths.

The room temperature EPR line shape reflects the mobility of the spin label side chain that depends on its topographical location. The term "mobility" is used in a general sense, and it includes effects on the spectra because of the motional rate, amplitude, and anisotropy of the nitroxide reorientation, characterizing the motional freedom of the nitroxide in the nanosecond time scale. Interactions between the nitroxide and neighboring side chains or backbone atoms may restrict its mobility, thus causing a broadening of the EPR lines and an increase in the apparent hyperfine splitting. Strong interactions result in a powder-like spectral pattern with a resolved high field hyperfine line and a large hyperfine splitting in the spectrum (for example see position *78* in Fig. 3, *right panel*). On the contrary, weak interactions between the nitroxide and the rest of the protein, as found for helix surface sites or loop regions, result in narrowing of the EPR lines and a decrease of the apparent hyperfine splitting in the spectra (for example see position *88* in Fig. 3, *right panel*). In addition, protein backbone dynamics contribute to the overall mobility of the spin label side chain. Dynamic domains exhibit very high mobility values, and the EPR spectral features resemble those of a free spin label in viscous solutions (for example see positions *98* and *122* in Fig. 3, *right panel*). The mobility can be quantified via the parameter ΔH_0^{-1} which is the inverse line width of the central resonance line (29). The resulting mobility profile is shown in Fig. 4*A*.

All residues located in the transmembrane region of the complex (Val^{78}–Leu^{82}) and the following residues up to Ala^{87} are characterized by low mobility values ($\sim$1.5 mT^{-1}), suggesting a close packing of the complex up to position 87. From residues Ala^{88} to Ala^{94} the R1 side chain mobility gradually increases and finally reaches very high values ($\sim$4.5 mT^{-1}) in the Ala^{95}–Gly^{101} region, which clearly point to the presence of a very dynamic AS-1 C-terminal end lacking fixed structural features. The mobility profile of Fig. 4*A* reveals a periodicity of the ΔH_0^{-1} values up to position 94; however, the periodicity pattern is not directly commensurable with a canonical α-helix.

The residues investigated in the predicted charged region connecting AS-1 and AS-2 also show a lack of a rigid structure and of close tertiary interactions with neighboring residues (positions 105, 106, 115, and 116). Positions 122 in the AS-2 sequence (*f* in the heptad repeat) and 148 show as well spectra characterized by high mobility.

Accessibility measurements were performed to distinguish residues exposed to the water or lipid phases or buried in the protein interior. The collision frequency between the nitroxide and the water-soluble CrOx is negligible for side chains not exposed to the bulk water. On the other hand, molecular oxygen allows us to distinguish between side chains oriented into the protein interior, showing a low collision frequency, and those directed into the lipid bilayer, exhibiting a high accessibility. The change in the electron longitudinal relaxation time (T_1) is a relative measure of the collision frequency between the nitroxide and the paramagnetic relaxing agent and can be determined by the method of continuous wave power saturation according to Altenbach *et al.* (23, 24).

Fig. 4*B* shows the accessibility data for the AS-1 region in terms of the dimensionless parameter Π, which is proportional to the collision frequency of the R1 side chain with either oxygen or CrOx. Low values for both Π_{CrOx} and Π_{Oxygen} are found for side chains up to position 86, showing a periodicity for Π_{Oxygen} typical for an α-helical secondary structure. It is worth noting the consistency between the low Π values observed characteristically for residues in a dense protein packing interface and the low mobility values measured for the same region. For positions 87–94 the Π_{CrOx} values gradually increase, in line with the notion that the side chains become more dynamic and more exposed to the bulk water. Accordingly, the Π_{Oxygen} values are also increasing. The periodicity observed in this region cannot be directly ascribed to a helical pattern, although it might be present. The reason for this failure to recognize possible secondary structure elements might be the fact that for interfacial regions the accessibility/mobility data lose their statistical significance (30). From positions 95 to 101, the Π_{CrOx} values approach those typical for water-exposed residues. Most interestingly, the decreased CrOx accessibility observed in the water-exposed region at positions 97 and 98 suggests possible interactions with neighboring residues that can hinder the CrOx diffusion toward the spin label attached at those sites. The almost constant level of Π_{Oxygen} ($\sim$0.6) obtained for positions 91–101 is indicative of nitroxides exposed to the aqueous phase.

The mobility and accessibility data for the predicted AS-1 sequence in the HAMP domain demonstrate its gradual protrusion from the transmembrane region to the aqueous phase. Moreover, the data enabled us to distinguish among three segments within the 83–101 sequence: the first (Gly^{83}–Ala^{87}) characterized by helical periodicity and close contact with neighboring residues; the second (Ala^{88}–Ala^{94}) still characterized by a periodical pattern and intermediate in mobility located in the membrane adjacent region; and the third (Ala^{95}–Gly^{101}) exposed to the bulk aqueous phase lacking fixed structural features.

Polarity Measurements—The A_{zz} parameters obtained from the low temperature spectra of the positions under investigation in the HAMP

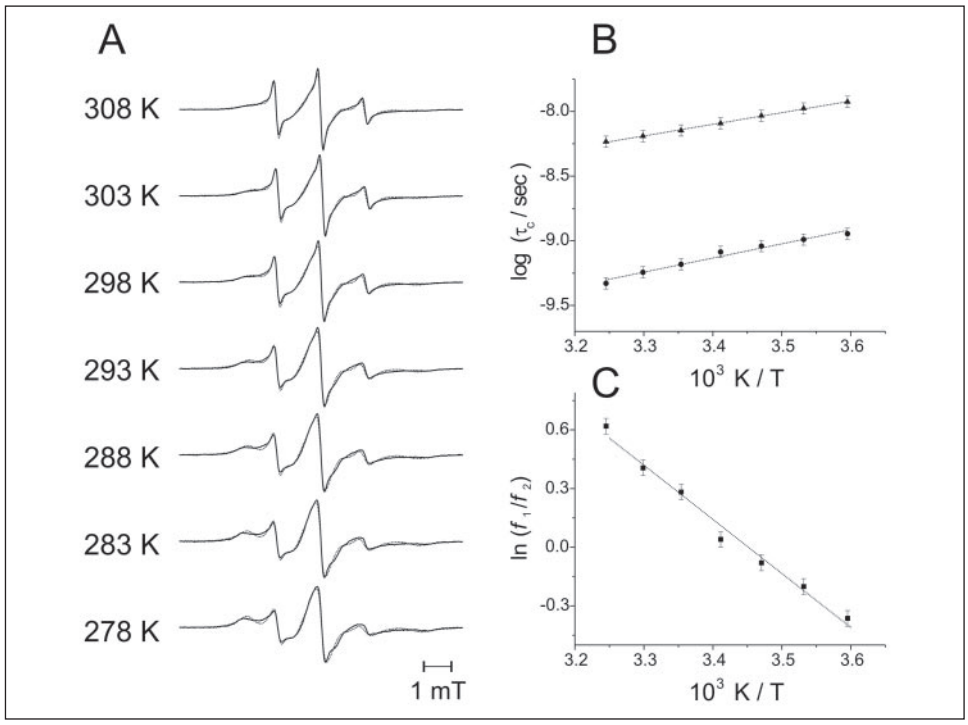

FIGURE 5. **Temperature effects on the spectral features of the spin-labeled NpHtrII$_{157}$ in complex with NpSRII reconstituted in PML.** *A,* the EPR spectra of NpSRII/NpHtrII-S91R1 determined at different temperatures (*black lines*) are presented. Fitting of the experimental spectra (*dotted lines*) performed to obtain the ratio of the two components are superimposed (see "Experimental Procedures"). *B,* plot of the logarithm of τ_c obtained from the fitting of the two components *versus* the inverse temperature (component 1, mobile (*black circles*); component 2, less mobile (*black triangles*)). The linear interpolation of the data leads to the following values for the slope: $(1.1 \pm 0.1) \times 10^3$ K (component 1); $(0.90 \pm 0.01) \times 10^3$ K (component 2). *C,* plot of the natural logarithm of the ratio of the fractions of the two components ($K = f_1/f_2$) *versus* the inverse temperature. The reaction entropy and enthalpy values determined from the intercept and the slope of the regression line amount to 80 J·mol^{-1}·K^{-1} and 23 kJ·mol^{-1}, respectively. The value of the equilibrium constant *K* calculated at 298.15 K is 1.30.

domain are presented in Fig. 4*C* and compared with the mobility and accessibility data already presented. The gradual increase of the A_{zz} values from positions 78 to 94 confirms that the first part of the AS-1 sequence is protruding from the protein/protein interface into a more polar aqueous environment, in agreement with the findings based on mobility and accessibility data. The third segment in the AS-1 sequence (positions 95–101), which has been shown to be a very dynamic region exposed to the bulk water phase, is indeed characterized by higher A_{zz} values up to 3.60 mT for positions 95 and 101. However, for those residues fully exposed to water, the expected values should be in the 3.6–3.7 mT range (26, 27), as observed for positions 105, 115, and 122 in the following region. Lowering the temperature might favor a more compact packing of the transducers in the complex, as already suggested by the decrease of the fraction of the mobile component in the spectra (Fig. 5*A*). This fact could explain the relatively low polarity values obtained for the dynamic region of the AS-1 sequence. Nevertheless, the trend of the A_{zz} values *versus* residue number reflects the Π_{CrOx} profile, with a remarkable decrease in both polarity and water accessibility around positions 94 and 97. This clearly indicates the presence of a similar topology of the transducer in the complex at room and low temperatures.

Temperature Effects on the EPR Spectral Features—To investigate the molecular origin of the presence of two spectral components in the room temperature EPR spectra, we analyzed the spectra in terms of a two-state equilibrium model, in which the HAMP domain is engaged in different conformational states characterized by different dynamic properties. A series of EPR spectra for NpSRII/NpHtrII-S91R1 were recorded at different temperatures between 278 and 308 K in steps of 5 K. From the fitting of simulated spectra to the experimental ones (see "Experimental Procedures"), it was possible to determine the fractions of the two components in each spectrum. The spectra and the corresponding fittings are presented in Fig. 5*A*. The two effective rotational correlation times (τ_c) for each spectrum were allowed to vary in accordance with temperature. The logarithm of the values obtained for the τ_c *versus* the inverse temperature is presented in Fig. 5*B*. The similar slope

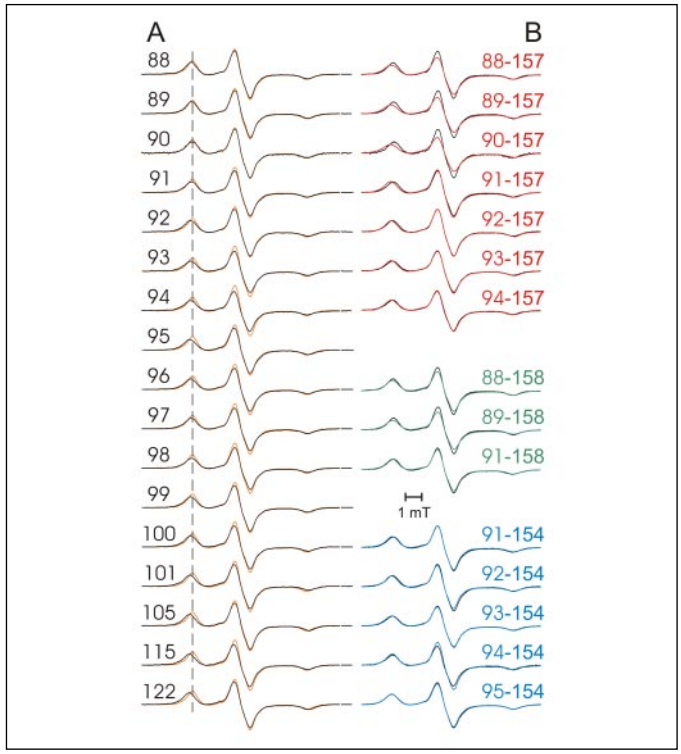

FIGURE 6. **Low temperature ($T = 160$ K) EPR spectra of singly labeled transducer and doubly labeled receptor-transducer complexes.** *A,* spin normalized EPR powder spectra of spin-labeled NpHtrII$_{157}$ in complex with NpSRII reconstituted in PML (*black line*) compared with a reference spectrum without dipolar broadening (*orange line*, see "Experimental Procedures"). The strength of the dipolar interaction and the resulting broadening are visible by the difference between the central amplitude of spin-normalized spectra with that of the reference spectrum. Changes in the A_{zz} parameter can be easily visualized with respect to the position of the low field line of the reference spectrum ($A_{zz} = 3.44$ mT), indicated by the *dashed vertical line. B,* spin normalized EPR powder spectra of doubly spin-labeled NpSRII/NpHtrII$_{157}$ reconstituted in PML (*colored line*) compared with the spectra of the respective singly spin-labeled NpHtrII$_{157}$ in the 2:2 complex (*black line*).

TABLE ONE

Transducer-transducer and transducer-receptor interspin distances in the NpSRII/NpHlrII$_{157}$ 2:2 complex

Interspin distances in the 2:2 complex reconstituted in PML were obtained from the simulations of low temperature spectra of singly labeled NpHtrII$_{157}$ and doubly labeled NpHtrII$_{157}$ and NpSRII (see "Experimental Procedures"). The estimated error is ±0.1 nm for all given distances. The distances determined from the simulations of the spectra of doubly labeled mutants in the transducer and in the receptor are compared with those determined for the singly labeled mutants in the transducer to obtain the extent of the receptor/transducer interaction (given in parentheses).

NpHtrII$_{157}$R1 position	Interspin distance			
	NpHtrII′$_{157}$ (analogous R1 position)	NpSRII (K157R1)	NpSRII (S158R1)	NpSRII (S154R1)
	nm	*nm*	*nm*	*nm*
88	>2.0	1.6 (1.6)	1.7 (1.7)	
89	>2.0	1.5 (1.5)	1.6 (1.6)	
90	>2.0	1.4 (1.4)		
91	1.9	1.9 (>2.0)	1.8 (>2.0)	
92	1.9	>2.0 (>2.0)		~2.0 (>2.0)
93	1.7	1.8 (>2.0)		1.7 (>2.0)
94	1.8	1.7 (>2.0)		~2.0 (>2.0)
95	1.8			1.8 (>2.0)
96	1.8			
97	1.8			
98	1.9			
99	1.9			
100	1.7			
101	1.9			
105	>2.0			
115	1.8			
122	1.9			

of both lines is evidence for similar activation energies for the reorientational motion of the nitroxide in both states. Analysis of the spectral component ratios revealed an increase of the less mobile component from 31 to 53% by decreasing the temperature from 308 to 278 K. The natural logarithm of the equilibrium constant for the transition between the two conformations exhibits a linear dependence with the inverse temperature (Fig. 5*C*). Entropy and enthalpy values determined from the intercept and the slope of the regression line amount to 80 J·mol^{-1}·K^{-1} and 23 kJ·mol^{-1}, respectively.

Spin-Spin Interactions and Distance Determination—In order to analyze spin-spin interactions in the dimeric receptor-transducer complex, low temperature spectra of singly labeled transducers are compared with a standard reference spectrum characterized by the absence of dipolar broadening (see "Experimental Procedures" and Fig. 6*A*). In the 88–94 region of the AS-1 sequence, interspin interactions are detectable starting from position 91 (1.9 nm) and become more evident for positions 93 and 94 where the fitting of the simulated spectra to the experimental ones yields distance values of 1.7–1.8 nm (TABLE ONE). This finding is in agreement with the decrease in the polarity and in the CrOx accessibility observed for positions 93 and 94 (see Fig. 4, *B* and *C*). It is worth noting that in the case of a straight continuation of the TM2 helix perpendicular to the membrane, positions 93 and 94 are expected to be located within the interface between the neighboring transducers but should not show stronger interactions than those observed for positions 89 and 90. The fact that closer contacts are observed for positions 93 and 94 indicates a possible inclination of the membrane adjacent part of the transducers toward each other.

Despite the highly dynamic nature of the region 95–101, the two transducers interact with each other in the complex showing distances in the 1.8 nm range. The lack of periodicity in the distances is to be expected because of the dynamic properties of this region. The analysis of three additional sites within the HAMP domain (Leu^{105}, Asp^{115}, and Ala^{122}) reveals close contact between positions 115 and 115′ and 122 and 122′ (TABLE ONE). This is a clear indication that despite the high dynamic properties of this region structural elements can be discerned.

To investigate the relative orientation of the AS-1 sequence of NpHtrII with respect to the cognate NpSRII, distance measurements between residues at the cytoplasmic end of helix F (K157R1, S158R1) and positions 88–94 of the transducer were performed. Additionally, proximity relations between S154R1, located at the cytoplasmic edge of helix F in the receptor, and positions 91–95 in the transducer have been determined. It has to be pointed out that the system under investigation is a complex of four proteins, and a double mutation involving the receptor and the transducer leads to several spin-spin interactions. In particular, dipolar interactions between both receptor-transducer and transducer-transducer positions can lead to the appearance of dipolar broadening in the low temperature continuous wave EPR spectra.

In order to focus only on the dipolar broadening because of the receptor-transducer interaction, the spectra of the doubly labeled variants are superimposed to the spectra of the respective singly labeled transducer. The additional decrease in intensity in the spin normalized spectra presented in Fig. 6*B* indicates the presence of considerable dipolar interaction between the spin-labeled transducer-receptor positions.

The closest distances to K157R1 are observed for positions 88–90 (TABLE ONE), whereas position 91, which is located one turn up in the helical structure suggested, shows just weak dipolar interactions, corresponding to a distance >2 nm. In agreement with these findings, the closest distances to S158R1 are observed for positions 88 and 89, whereas the double mutant NpSRII-S158R1/NpHtrII-S91R1 shows weak interactions as well. These observations are in line with an α-helical arrangement of these residues where the helical turn 88–90 is located in the vicinity of residues Lys^{157}–Ser^{158} in helix F. An ideal prolongation of helix TM2 is in agreement with these data. Based on this assumption, the same strength of spin-spin interactions is expected for the following positions 91–95 and S154R1, located one helix turn above Lys^{157} and Ser^{158}. However, the spectra obtained for these doubly

labeled variants do not show any additional broadening with respect to the singly labeled transducers, thus indicating a more complex topology of the transducer dimer. Hence, the AS-1 region following residue Ser^{91} is in closer contact to the neighboring transducer rather than to the receptor, corroborating the conclusions drawn from the distance values determined from the singly labeled transducers.

DISCUSSION

Four different parameters accessible by EPR were determined to elucidate the structural properties of the membrane proximal linker region of the transducer in complex with NpSRII.

Adjacent to residue Leu^{82}, which is the last amino acid for which electron density could be determined by x-ray crystallography (6), follows the first amphipathic sequence AS-1 of the HAMP domain. Within this AS-1 sequence (Gly^{83}–Gly^{101}) three segments characterized by different tertiary contacts and dynamic properties could be identified.

The clear periodicity of 3.6 residues revealed by the oxygen accessibility from positions 78 to 87 strongly suggests that this part of AS-1 is the α-helical extension of TM2. Moreover, the low R1 side chain mobility observed for positions 78–87 indicates tertiary contacts with neighboring residues, which is also corroborated by the periodical pattern of oxygen accessibility. Most interestingly, the higher oxygen accessibility values are observed for the positions oriented toward NpSRII, indicating a dense packing of residues in the transducer/transducer interface.

The second segment of AS-1 (Ala^{87}–Ala^{94}) is proposed to be structured, because of the pattern observed in the mobility and accessibility values. Additionally, the close interactions observed between positions 88 and 90 and K157R1 and S158R1 in helix F in the receptor support the idea of a helical prolongation of TM2. The intermediate mobility values and the observed spin-spin interactions with the receptor residues suggest tertiary contacts with neighboring residues. The gradual increase of the average motional dynamics and of the accessibility toward CrOx provides strong evidence that this is the first region of the transducer protruding out of the protein/protein interface into the cytoplasmic phase.

The third segment of AS-1 (Ala^{95}–Gly^{101}) of $NpHtrII_{157}$ is characterized by completely different dynamic and structural properties. The lack of a fixed structure starting from position 95 is strongly supported both by mobility and accessibility analysis. The results favor a model in which the helical predicted AS-1 sequence ends at Ala^{94} and the connector dynamic region of undefined structure exposed to the cytoplasmic water phase starts at Ala^{95}. The lack of fixed structural features and close tertiary contacts is also observed for the four residues in the following connector region up to position 116.

The AS-1 sequence investigation in terms of interspin interaction (Ala^{88}–Gly^{101}) defines vicinity relations between neighboring AS-1 sequences in the 2:2 complex. The spin-spin interactions are more pronounced for the 93–101 than for the preceding 88–92 positions. This is clear evidence for an inclination of the AS-1 sequences toward each other. Also in line with this conclusion are the close vicinity relations (1.4–1.6 nm) found between K157R1 and S158R1 in the cytoplasmic edge of helix F in the receptor and positions 88–90 in the AS-1 sequence. In fact, a previous EPR study (12) determined similar distances (1.4–1.5 nm) between S158R1 and positions 80 and 81, which are located two helical turns down in TM2. In the case of AS-1 being a simple straight prolongation of TM2, one would have expected much closer interactions between S158R1 and the 88–90 region than those actually detected.

These findings, together with the absence of spin-spin interactions between S154R1, located one helix turn up toward the cytoplasmic EF loop in the receptor, and positions 91–95 in the AS-1 sequence, further suggest a model of an inclination of the transducers in the membrane adjacent region to a direction opposite to the receptor, leading to the formation of a loose coiled-coil motif.

The vector representation of the CrOx accessibility values obtained for the proposed α-helical part of the AS-1 sequence (Ala^{88}–Ala^{94}) further confirms the tilting of this domain toward the central axis of the complex (Fig. 7*B*). The loose coiled-coil motif proposed also accounts for the pronounced reduction of CrOx accessibility observed around positions 93 and 97 (located at positions d and a, respectively, in the proposed heptad repeats).

The presence of Gly^{83} and Gly^{84}, two putative helix-breaking residues, might induce the proposed distortion in the helical axis of the AS-1 sequence leading to structural flexibility. Cysteine substitution at position 83 has been shown to completely eliminate phototaxis without impairing the affinity of the transducer toward the receptor, whereas the second glycine residue at position 84 can be replaced without loss of function (31). It should be noted that the presence of helix breaking elements in the 83–89 region (numbering according to NpHtrII, see Fig. 1) is a general feature of HAMP domains (5).

The topology proposed here for the AS-1 sequence is overall in line with the model recently proposed by Spudich and co-workers (17) for the solubilized NpSRII-NpHtrII complex, where the membrane proximal domain up to residue 95 was suggested to interact with the EF loop of the receptor. The discrepancies related to the inclination of the transducer might be due to the different technique and sample used. The data presented here concerns the 2:2 complex reconstituted in the membrane, and it has been proven that solubilization induces structural changes in the interfacial region under investigation.[6]

Fig. 7, *C* and *D*, combines all the information available for the AS-1 sequence of the HAMP domain in the predicted EPR model up to position 101. The connector region is also modeled in an extended conformation, although from the limited number of positions investigated, it is not possible to extract more precise topological details. An analogous study performed on the HAMP domain of the aspartate chemoreceptor (Tar) via disulfide scanning (32) also showed that the connector region between the two identified helical segments AS-1 and AS-2 was lacking any kind of periodicity in the solvent exposure pattern. Even though it was suggested that this region is at least partially buried, and it does not appear to be located at the dimer interface, the authors suggested that it must not be a simple extension of AS-1.

The dynamics observed in the HAMP domain do not exclude the presence of defined secondary structure and tertiary contacts as supported by the close distances observed between highly mobile side chains found in AS-1, connector, and AS-2. The AS-2 sequence is tentatively proposed to start the α-helical coiled-coil dimer because of the interactions (1.9 nm) detected between A122R1 and A122′R1 (position f in the heptad repeats). An EPR analysis performed on in-parallel in-register coiled-coil vimentin dimers showed that residues located at the buried sites a and d reveal strong interactions (1.0–1.5 nm), whereas non a/d residues are widely separated (>2 nm) on the outside of the helical bundle (33).

The following question arises. How does the signal propagate from the activated TM2 helix in the transmembrane region through the HAMP domain up to the tip of the cytoplasmic coiled-coil region? The highly dynamic nature of the linker region reveals insight into the signal transfer mechanism. The low polarity values determined for the

[6] J. P. Klare, Bordignon, E., Doebber, M., Fitter, J., Kriegsmann, J., Chizhov, I., Steinhoff, H.-J., and Engelhard, M., submitted for publication.

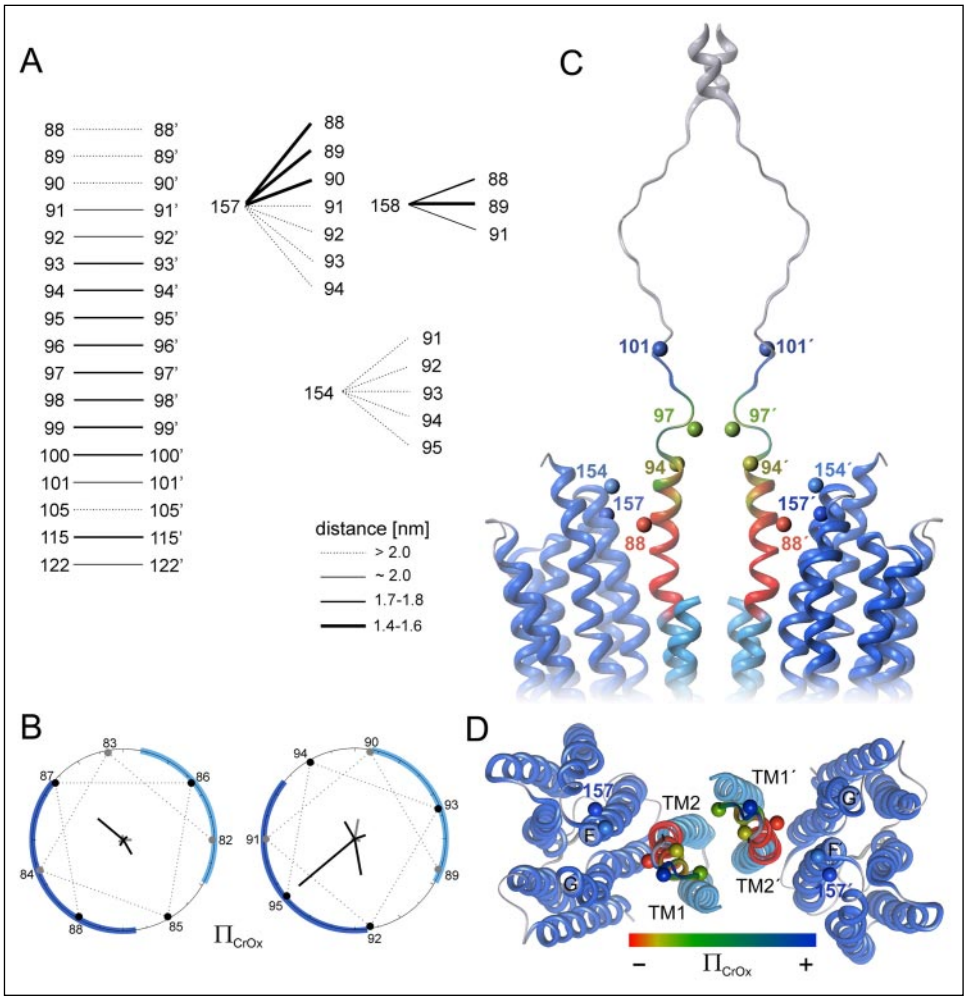

FIGURE 7. **Model of the membrane adjacent region of NpHtrII$_{157}$ in complex with NpSRII reconstituted in PML based on EPR data.** *A,* schematic representation of the trend of distances obtained between all the positions investigated used as topological constraints for the model (the values depicted for the transducer-receptor interactions are those estimated in *parentheses* in TABLE ONE). *B,* vector analysis of the accessibility parameters for positions 82–94 in the proposed α-helical arrangement. The residues in the proposed helical structure oriented toward the cognate receptor or transducer are highlighted in *blue* and *cyan,* respectively. The *left wheel* shows the first two helical turns protruding out of helix TM2 (82–84, *gray*; 85–88, *black*) and the *right wheel* depicts the following two helical turns (89–91, *gray*; 92–95, *black*). The length of the lines pointing to the respective residue is proportional to the Π_{CrOx} value obtained for that position; the Π_{CrOx} values for the left wheel have been multiplied by 10 for better comparison. The low accessibility values in the left wheel indicate the presence of tertiary interactions up to residue Ala^{88}. In the right wheel, the first turn is shown to have higher accessibility to CrOx in the transducer/transducer interface, whereas the second turn shows clearly higher accessibility to CrOx for residues directed toward the receptor, according to the proposed inclination of the transducers toward each other. *C,* side view of the HAMP domain model up to position 125. The NpSRII-NpHtrII transmembrane complex obtained from the x-ray data is depicted as *blue* (NpSRII) and *cyan* (NpHtrII) ribbon representation. The AS-1 sequence proposed by EPR data is colored according to the accessibility to CrOx (see legend at the bottom of the figure). C-β atoms from selected residues are represented as *balls* colored according to the Π_{CrOx} values. The AS-1 segment from Gly^{83} to Ala^{94} is proposed to be the helical extension of TM2. To account for the high dynamic properties observed, the Ala^{95}–Gly^{101} segment is represented in an extended conformation, although from the EPR data a highly dynamic helical segment cannot be excluded. A structural kink is proposed at residue Gly^{83} that leads to the loose coiled-coil motif suggested. The *gray* region of the HAMP domain (Asp^{102}–Asp^{125}) is presented for illustrative purposes only because no further structural information is available. The extended conformation chosen to represent the connector region up to residue 116 (*gray line*) accounts for its dynamic properties, whereas the AS-2 sequence is tentatively proposed to start the coiled-coil superstructure. *D,* top view from the cytoplasmic side of the model up to residue Gly^{101}.

dynamic part of the AS-1 sequence and the decrease of the fraction of the more mobile spectral component upon lowering the temperature suggest that changes in temperature can modify the dynamics of the HAMP domain. It is also suggested that the HAMP domain exists in equilibrium between two conformations that differ in their dynamic properties. This is revealed by the presence of two spectral components through all the HAMP domain positions investigated so far. These findings may account for the absence of structural data in the x-ray analysis for the residues beyond position 82 (6).

Furthermore, it is shown that the presence of both the cognate transducer and the membrane bilayer introduces stabilization constraints for the arrangement of the HAMP domain.[6] Solubilization of the complex is in fact disrupting the transducer-transducer dimer and inducing structural changes in the membrane adjacent region of the transducer. Finally, a preliminary EPR analysis of selected positions in the AS-1 sequence of NpSRII/NpHtrII$_{157}$ reconstituted in PML suspended in buffer with a high NaCl concentration reveals a general restriction of the side chain mobility induced by salt (data not shown). This is a clear indication that salt affects the HAMP domain structure and dynamics. The presence of high salt concentration (up to 4 M) in the natural environment of halobacteria therefore seems to be of importance for the stability and function of the HAMP domain, as it has been already observed for halophilic enzymes (34).

The relatively facile modulation of the HAMP domain dynamics exerted by environmental input suggests the means how small changes in TM2 (screw-like motion (3, 12, 35)) can trigger the physiological response. How the structural changes observed in TM2 after light excitation can propagate along the transducer, either inducing a new con-

formational/dynamic state in the HAMP domain or shifting a pre-existing equilibrium between the active/inactive conformations, is currently under investigation by means of SDSL EPR. Changes in the dynamic properties of the receptor/transducer upon activation/deactivation may be the "language" of signal transduction for chemoreception and photoreception as put forward by Kim *et al.* (36).

Acknowledgments—We thank C. Beier for help with the modeling and visualization of the HAMP domain and A. Göppner for technical assistance.

REFERENCES

1. Tomioka, H., Takahashi, T., Kamo, N., and Kobatake, Y. (1986) *Biochem. Biophys. Res. Commun.* **139,** 389–395
2. Spudich, J. L., Yang, C.-S., Jung, K.-H., and Spudich, E. N. (2000) *Annu. Rev. Cell Dev. Biol.* **16,** 365–392
3. Klare, J. P., Gordeliy, V. I., Labahn, J., Büldt, G., Steinhoff, H. J., and Engelhard, M. (2004) *FEBS Lett.* **564,** 219–224
4. Aravind, L., and Ponting, C. P. (1999) *FEMS Microbiol. Lett.* **176,** 111–116
5. Williams, S. B., and Stewart, V. (1999) *Mol. Microbiol.* **33,** 1093–1102
6. Gordeliy, V. I., Labahn, J., Moukhametzianov, R., Efremov, R., Granzin, J., Schlesinger, R., Büldt, G., Savopol, T., Scheidig, A. J., Klare, J. P., and Engelhard, M. (2002) *Nature* **419,** 484–487
7. Appleman, J. A., and Stewart, V. (2003) *J. Bacteriol.* **185,** 89–97
8. Kim, K. K., Yokota, H., and Kim, S.-H. (1999) *Nature* **400,** 787–792
9. Jung, K.-H., Spudich, E. N., Trivedi, V. D., and Spudich, J. L. (2001) *J. Bacteriol.* **183,** 6365–6371
10. Trivedi, V. D., and Spudich, J. L. (2003) *Biochemistry* **42,** 13887–13892
11. Wegener, A. A., Chizhov, I., Engelhard, M., and Steinhoff, H.-J. (2000) *J. Mol. Biol.* **301,** 881–891
12. Wegener, A. A., Klare, J. P., Engelhard, M., and Steinhoff, H.-J. (2001) *EMBO J.* **20,** 5312–5319
13. Klare, J. P., Bordignon, E., Engelhard, M., and Steinhoff, H.-J. (2004) *Photochem. Photobiol. Sci.* **3,** 543–547
14. Sudo, Y., Iwamoto, M., Shimono, K., Sumi, M., and Kamo, N. (2001) *Biophys. J.* **80,** 916–922
15. Schmies, G., Engelhard, M., Wood, P. G., Nagel, G., and Bamberg, E. (2001) *Proc. Natl. Acad. Sci. U. S. A.* **98,** 1555–1559
16. Hippler-Mreyen, S., Klare, J. P., Wegener, A. A., Seidel, R., Herrmann, C., Schmies, G., Nagel, G., Bamberg, E., and Engelhard, M. (2003) *J. Mol. Biol.* **330,** 1203–1213
17. Yang, C. S., Sineshchekov, O., Spudich, E. N., and Spudich, J. L. (2004) *J. Biol. Chem.* **279,** 42970–42976
18. Chen, X., and Spudich, J. L. (2004) *J. Biol. Chem.* **279,** 42964–42969
19. Hohenfeld, I. P., Wegener, A. A., and Engelhard, M. (1999) *FEBS Lett.* **442,** 198–202
20. Ho, S. N., Hunt, H. D., Horton, R. M., Pullen, J. K., and Pease, L. R. (1989) *Gene* (*Amst.*) **77,** 51–59
21. Shimono, K., Iwamoto, M., Sumi, M., and Kamo, N. (1997) *FEBS Lett.* **420,** 54–56
22. Pfeiffer, M., Rink, T., Gerwert, K., Oesterhelt, D., and Steinhoff, H.-J. (1999) *J. Mol. Biol.* **287,** 163–171
23. Altenbach, C., Greenhalgh, D. A., Khorana, H. G., and Hubbell, W. L. (1994) *Proc. Natl. Acad. Sci. U. S. A.* **91,** 1667–1671
24. Altenbach, C., Marti, T., Khorana, H. G., and Hubbell, W. L. (1990) *Science* **248,** 1088–1092
25. Steinhoff, H.-J., Radzwill, N., Thevis, W., Lenz, V., Brandenburg, D., Antson, A., Dodson, G., and Wollmer, A. (1997) *Biophys. J.* **73,** 3287–3298
26. Steinhoff, H.-J., Savitsky, A., Wegener, C., Pfeiffer, M., Plato, M., and Möbius, K. (2000) *Biochim. Biophys. Acta* **1457,** 253–262
27. Plato, M., Steinhoff, H.-J., Wegener, C., Törring, J. T., Savitsky, A., and Möbius, K. (2002) *Mol. Phys.* **100,** 3711–3721
28. Fried, J. P. (1976) in *Spin Labeling: Theory and Applications* (Berliner, L. J., ed) pp. 83–91, Academic Press, New York
29. Hubbell, W. L., Mchaourab, H. S., Altenbach, C., and Lietzow, M. A. (1996) *Structure* **4,** 779–783
30. Cuello, L. G., Cortes, D. M., and Perozo, E. (2004) *Science* **306,** 491–495
31. Yang, C.-S., and Spudich, J. L. (2001) *Biochemistry* **40,** 14207–14214
32. Butler, S. L., and Falke, J. J. (1998) *Biochemistry* **37,** 10746–10756
33. Hess, J. F., Voss, J. C., and FitzGerald, P. G. (2002) *J. Biol. Chem.* **277,** 35516–35522
34. Lanyi, J. K. (1974) *Bacteriol. Rev.* **38,** 272–290
35. Chervitz, S. A., and Falke, J. J. (1996) *Proc. Natl. Acad. Sci. U. S. A.* **93,** 2545–2550
36. Kim, S. H., Wang, W., and Kim, K. K. (2002) *Proc. Natl. Acad. Sci. U. S. A.* **99,** 11611–11615